

Research Paper

Hybrid micelles containing methotrexate-conjugated polymer and co-loaded with microRNA-124 for rheumatoid arthritis therapy

Fei Hao¹, Robert J Lee^{1,2}, Lihuang Zhong¹, Shiyang Dong¹, Chunmiao Yang¹, Lirong Teng¹, Qingfan Meng¹, Jiahui Lu¹, Jing Xie¹, Lesheng Teng¹✉

1. School of Life Sciences, Jilin University, No.2699, Qianjin Street, Changchun130012, P.R. China
2. College of Pharmacy, The Ohio State University, Columbus, 500 W 12th Ave, Columbus, OH 43210, USA

✉ Corresponding author: Lesheng Teng, Ph.D., Professor, School of Life Sciences, Jilin University, No.2699, Qianjin Street, Changchun, China, 130012, Tel: (86) 13844181693; Email: tenglesheng@jlu.edu.cn.

© The author(s). This is an open access article distributed under the terms of the Creative Commons Attribution License (<https://creativecommons.org/licenses/by/4.0/>). See <http://ivyspring.com/terms> for full terms and conditions.

Received: 2018.12.14; Accepted: 2019.05.29; Published: 2019.07.09

Abstract

Purpose: Methotrexate (MTX) is a first-line drug for rheumatoid arthritis (RA) therapy. However, MTX monotherapy often results in irreversible joint damage due to its slow onset of action and long duration. microRNA-124 (miR-124) has shown direct bone protection activity against RA. A co-delivery system for MTX and microRNA combination may provide therapeutic synergy.

Methods: Methotrexate-conjugated polymer hybrid micelles (M-PHMs) were prepared by self-assembly of two functional amphiphilic polymers (MTX-PEI-LA and mPEG-LA) at an optimized weight ratio. Incorporation of microRNA was achieved through electrostatic interactions between microRNA and cationic polymer MTX-PEI-LA. Cellular uptake, endosome escape, biodistribution, and therapeutic efficacy of M-PHMs/miR-124 complexes were investigated and evaluated in RAW264.7 cells and a rat adjuvant-induced arthritis (AIA) model.

Results: M-PHMs/miR-124 complexes exhibited folate receptor-mediated uptake in activated RAW264.7 cells. miR-124 was able to escape from the endosome and down-regulate nuclear factor of activated T cells cytoplasmic 1 (NFATc1). M-PHMs/miR-124 complexes accumulated in inflamed joints of AIA rats and showed superior therapeutic efficacy through both anti-inflammatory effect and direct bone protective effect. Combination of miR-124 and MTX in these micelles induced disease remission.

Conclusions: M-PHMs/miR-124 was highly effective against RA through therapeutic synergy. Additional studies are warranted to further investigate its therapeutic potential and delineate its mechanisms of action.

Key words: polymeric hybrid micelles, folate receptor, methotrexate, microRNA-124, rheumatoid arthritis

Introduction

Rheumatoid arthritis (RA) is a complex and incurable chronic autoimmune disease with multiple mechanisms of pathogenesis [1, 2]. Disease-modifying antirheumatic drugs (DMARDs) are used for the treatment of RA. However, a monotherapy usually cannot achieve sustained and complete disease remission [3, 4]. Accordingly, new treatments

are urgently needed [5]. Combination therapy of DMARDs and biomacromolecules such as siRNA [6, 7], microRNA [8, 9], and monoclonal antibody [10, 11] is a promising approach [4, 12]. Methotrexate (MTX) is a frequently used DMARD and as the anchor drug for RA treatment [13, 14]. However, MTX monotherapy often results in drug resistance and

irreversible joint damage due to its slow onset of action and long duration [15-18]. MTX combination with biomacromolecules therapy is under intense investigation [19-22]. MicroRNAs are highly conserved sequences and post-transcriptional regulators of gene expression and are emerging as a novel therapeutic modality [8, 9, 23]. Each microRNA usually consists of 19-24 nucleotides and can simultaneously regulate multiple targets associated with disease [9, 24]. MicroRNA-124 (miR-124) recently has been identified as an RA-associated microRNA and a potential therapeutic target for RA treatment [25, 26]. pre-miR-124 injected into the joints of adjuvant-induced arthritis (AIA) rat model has been shown to effectively reduce bone destruction and osteoclast genesis [27]. MTX and miR-124 combination therapy maybe more effective against RA [28].

Nanoparticle-based therapy of RA has received much attention in recent years [29-31]. To increase the stability, reduce the off-target effects, and efficiently deliver both miR-124 and MTX to the specific targeting tissue, it is desirable to develop a targeted nanoparticle delivery system [31]. Activated macrophages have recently been reported as a promising target for RA nanotherapeutics. Receptors including folate receptor beta (FR β), scavenger receptor (SR), and hyaluronic acid receptor (CD44) are elevated in these cells [32-38]. Since FR β is not expressed in most normal tissues, drug carriers targeting FR β can be used to deliver drugs into these cells [32, 33, 39-47]. However, conventional FR-targeted delivery systems are often composed of distinct functional components for targeting and therapeutic activity [46]. Being able to combine both functions serves to simplify the composition of the delivery system, therefore, is desirable [31].

Polymer-drug conjugates have been used to increase drug solubility, alter drug pharmacokinetics, enhance drug therapeutic efficacy, and reduce systemic side-effects [48-50]. Furthermore, the drugs conjugated to polymers had great potential to achieve both therapeutic and targeted functions. Polymer-drug conjugates can form part of a multifunctional carrier for combination therapy [50, 51]. As a folic acid (FA) analog, MTX conjugated to polymers have recently been shown to target folate receptors [52-55]. MTX attached to generation 5 dendrimer (G5-MTX) via amide bond not only induced the cytotoxicity but greatly enhanced the affinity for folate receptor alpha (FR α) [53, 54]. Multivalent MTX was shown to bind FR α [56]. Recent studies showed that the amino groups of MTX play a key role in targeting FR α [57]. Most recently, studies have found that G5-PAMAM-FA-MTX has a stronger

FR β targeting effect compared to G5-PAMAM-FA [42]. Nakashima-Matsushita et al. reported that MTX could be transported to the synovial macrophages through FR β [58]. Qi et al. further demonstrated that G5-MTX was taken up by activated macrophages overexpressing FR β and had a similar anti-inflammatory effect as MTX at an equivalent dose [59]. Inspired by these findings, we hypothesized that MTX can be used to achieve efficient macrophage targeting and to exert therapeutic activity for RA.

Polyethylenimine(PEI) is a well-known non-viral cationic carrier for the delivery of nucleic acids, including siRNA and microRNA [60-62]. In addition, PEI can be used to construct a polymer-drug conjugate due to its abundance of amine functional group. PEI-drug conjugates can be further used for the delivery of oligonucleotides. Dong et al. prepared pre-functionalized polymer-drug conjugates for combination therapy of siRNA and chemotherapy drugs by coupling doxorubicin (DOX) and PEI [63]. Xu et al. also synthesized PEI-DOX for co-delivery of Bcl2 siRNA and DOX [64]. Both co-delivery systems exhibited a synergistic and enhanced antitumor efficacy.

In our previous study, it was shown that fatty acid, including oleic acid and linoleic acid, modified PEI exhibited a higher transfection efficiency for oligonucleotides and reduced cytotoxicity for normal cells [65, 66]. To achieve efficient co-delivery and combination therapy of microRNA and MTX with low carrier toxicity, MTX was first attached to linoleic acid modified branched PEI (MTX-PEI-LA). MTX-conjugated polymer hybrid micelles (M-PHMs) were self-assembled from a combination of MTX-PEI-LA and linoleic acid-modified methoxy-polyethylene glycol (mPEG-LA) and then complexed to miR-124, as illustrated in **Scheme 1A**. We proposed that M-PHMs/miR-124 could specifically target the activated macrophages in RA joints, successfully release the payloads into the cytoplasm, and achieve the combination therapy as shown in **Scheme 1B**.

Results and Discussion

Synthesis and characterization of MTX-PEI-LA and mPEG-LA

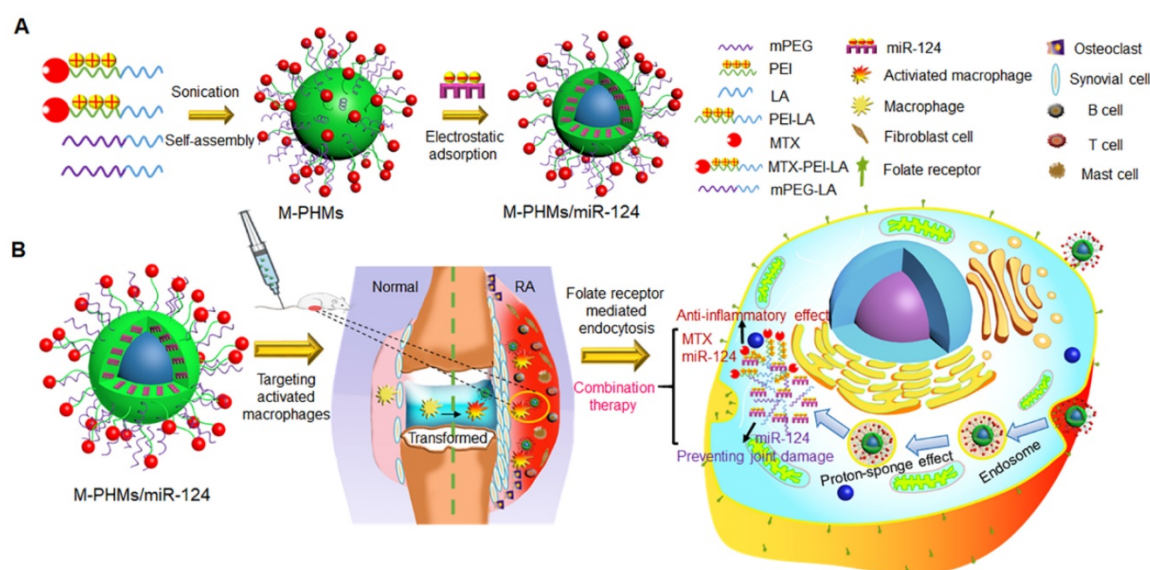
The synthesis procedure was shown in **Figure 1A** and chemical structures of the two amphiphilic polymers (MTX-PEI-LA and mPEG-LA) were confirmed by ¹H NMR and Fourier-transform infrared (FT-IR) spectra (**Figure 1B** and **Figure S1**). mPEG-2000 Da-NH₂ had a prominent peak at 3.62 ppm for methylene (a, 1 alpha-O-C and 1beta-O-C). Linoleyl chloride (LC) had prominent peaks at 5.35

ppm for 1-ethylene (b, 1-(C=C) or 1-C), 0.89 ppm for methyl (b1) and characteristic peaks at 2.88 ppm for methylene (b2, 1 α -C(C=O) Cl) in deuterated chloroform (CDCl₃). The characteristic peaks of PEI-25 kDa were also observed at 1.8-2.8 ppm (c) in CDCl₃. In the ¹H NMR spectra of mPEG-LA and PEI-LA (soluble in CDCl₃), the prominent peaks of mPEG-2000 Da-NH₂ (a), LC (b, b₁) and PEI-25 kDa (c) can be also found. However, the characteristic peak (b₂) of LC disappeared in the spectra of mPEG-LA and PEI-LA. This indicated that a chemical reaction had occurred and LC was successfully conjugated to mPEG-2000 Da-NH₂ and PEI-25 kDa. The characteristic peaks of MTX in ¹H NMR spectra were observed at 6.76 ppm (d) and 7.64 ppm (d₁) for 1-benzene, and 8.57 ppm (d₂) for 2-pyrazine in deuterated dimethyl sulfoxide (DMSO-d₆). In the ¹H NMR spectra of MTX-PEI-LA conjugates (dissolved in deuterated water(D₂O)), it not only contained the characteristic peaks of PEI-25 kDa (c), LC (b, b₁) but also the characteristic signals of MTX (d, d₁, d₂). MTX was successfully conjugated to PEI-LA. The characteristic peaks of aromatic protons in MTX conjugated with PEI-LA (d, δ =7.34; d₁, δ =7.71; d₂, δ =8.47) was a little offset. The peak shift may be induced by the reaction of MTX with PEI-LA. In FT-IR spectra, new peaks could be found at 3300-3500 cm⁻¹ in mPEG-LA (Figure S1A) and 3270 cm⁻¹ (Figure S1B) in PEI-LA due to the amide bond generation. As shown in Figure S1B, the characteristic peaks of the carboxyl group in MTX at 1602 cm⁻¹ and 1646 cm⁻¹ disappeared in MTX-PEI-LA [35]. All of this further confirmed that the MTX-PEI-LA and mPEG-LA were

successfully synthesized. MTX was conjugated to PEI-LA by an amide for several reasons. First of all, serum-stable amide provides greater stability in the blood [53]. Secondly, the MTX-conjugated polymers could be applied as a potential long-circulating formulation according to its stability. Finally, MTX-conjugated polymers may alter the pharmacokinetics and reduce the systemic toxicity of MTX. The absorption peak of MTX in MTX-PEI-LA was confirmed at 303 nm (Figure S2) and the drug loading efficiency were calculated to be 15.6%.

Formulation optimization for M-PHMs and M-PHMs/miR-124

M-PHMs were prepared by the self-assembly of MTX-PEI-LA and mPEG-LA. The properties of M-PHMs especially the cationic charge can be easily adjusted by changing the weight percentage of MTX-PEI-LA. As shown in Table S1, when the percentage of MTX-PEI-LA increased, the zeta potential of M-PHMs changed from negative to positive charge and the average size of M-PHMs also gradually increased. The particle sizes of M-PHMs with 5%, 10% and 20% of MTX-PEI-LA were all under 200 nm and had a narrow particle size distribution and low polydispersity index (PDI) (PDI < 0.25). Bovine serum albumin (BSA) precipitation assay was further conducted to assess the colloidal stability of M-PHMs with different percentages of MTX-PEI-LA in serum. As indicated in Figure S3, M-PHMs with 2% and 5% MTX-PEI-LA had a lower precipitation rate compared with M-PHMs with higher weight percentages of MTX-PEI-LA. The lower precipitation



Scheme 1. Schematic representation of MTX-conjugated polymer hybrid micelles co-loaded with miR-124 (M-PHMs/miR-124) preparation and combination therapy of M-PHMs/miR-124 in RA. (A) The M-PHMs were formed by the self-assembly of MTX-PEI-LA and mPEG-LA. miR-124 was then loaded through electrostatic interactions with the micelles. (B) M-PHMs/miR-124 targeted to the folate receptor (FR) on activated macrophages in RA joints and released MTX conjugates and miR-124 into the cytoplasm by the proton-sponge effect. The combination therapy had both anti-inflammatory effect and joint protective effect.

rate of M-PHMs demonstrated better stability in blood. In comparison with the M-PHMs (2% MTX-PEI-LA) with a negative zeta potential (-2.67 mV), M-PHMs (5% MTX-PEI-LA) with an appropriate positive zeta potential (7.57 mV) had a potential ability to form complexes with micro-RNA through electrostatic interactions. In summary, we chose to prepare M-PHMs composed of 5% MTX-PEI-LA and 95% mPEG-LA. In order to better characterize the M-PHMs properties, the polymer hybrid micelles (PHMs) without MTX conjugation were also prepared. The PHMs were comprised of PEI-LA and mPEG-LA and were set as a negative control for M-PHMs with potential targeted and therapeutic dual functions. The weight percentage of PEI-LA in PHMs

was also set as 5%. M-PHMs or PHMs referred in all of the following studies both represented a composition of 5% MTX-PEI-LA or 5% PEI-LA.

The morphology of MTX, MTX-PEI-LA, PHMs, and M-PHMs was further visualized by field emission scanning electron microscopy (FESEM) (**Figure 2A**). Compared with the crystal packing of free MTX, both MTX-PEI-LA, PHMs, and M-PHM formed uniform spherical particles in water. MTX-PEI-LA had a larger particle size than the M-PHMs and PHMs. Unlike the smooth surface of MTX-PEI-LA micelles, PHM and M-PHMs had a rough surface which may be caused by the polyethylene glycol (PEG) layer on the surface of nanoparticles due to its hydrophilicity. The critical micelle concentration (CMC) of PHMs (**Figure 2B**)

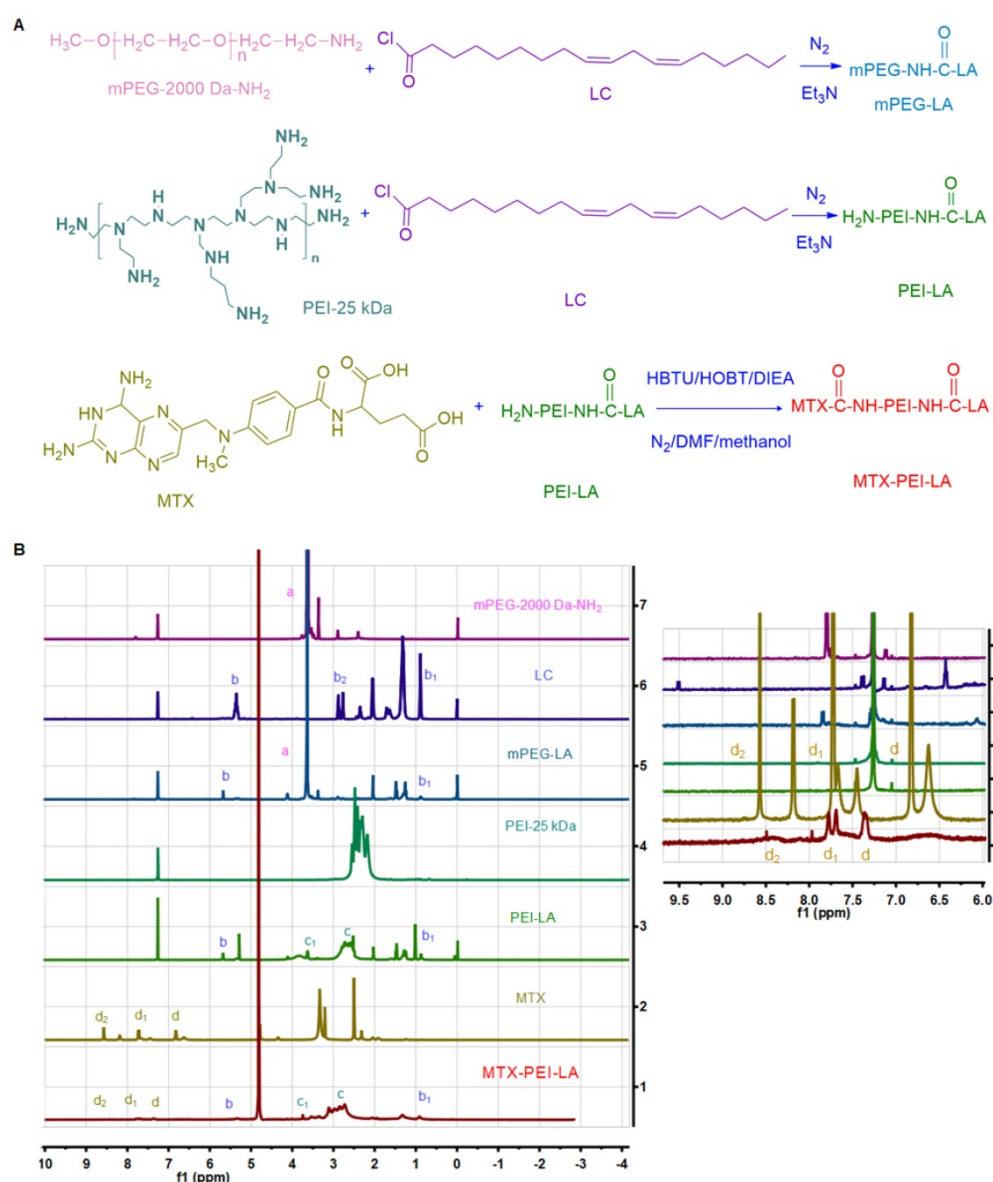


Figure 1. The chemical synthesis procedure and ¹H NMR spectrum of polymer conjugates. (A) Linoleyl chloride (LC) was first conjugated to the mPEG-NH₂ and PEI through the reaction of an acid chloride with an amine. MTX was then conjugated to the H₂N-PEI-LA through the acid and amine condensation reaction. (B) ¹H NMR spectrum (500 MHz) of mPEG-2000 Da-NH₂, LC, mPEG-LA, PEI-25 kDa, PEI-LA, MTX, MTX-PEI-LA. mPEG-2000 Da-NH₂, LC, PEI-25 kDa, mPEG-LA, and PEI-LA were dissolved in deuterated chloroform (CDCl₃). MTX was dissolved in deuterated dimethyl sulfoxide (DMSO-d₆). MTX-PEI-LA was dissolved in deuterated water (D₂O).

and M-PHMs (Figure 2C) were 10.0 $\mu\text{g}/\text{mL}$ and 6.28 $\mu\text{g}/\text{mL}$, respectively. M-PHMs and PHMs both had a lower CMC and may have good stability in blood circulation. Then the PHMs/miR-124 or M-PHMs/miR-124 complexes formed at differing nitrogen to phosphate ratios (N/P) were analyzed by 2% agarose gel electrophoresis. The N/P ratios of PHMs or M-PHMs to miR-124 were calculated based on the molar ratio of the N atoms in PEI-LA or MTX-PEI-LA composed of micelles (PHMs or M-PHM) to the negatively charged P groups of the miR-124 molecule. In PEI, each unit has a molecular weight of 43 and contains one N. In miR-124, each unit weight of 330 contains one P. In this study, PEI had been modified by LA and MTX. The degree of functionalization with PEI with LA and MTX was calculated to be 12 and 15, respectively, based on the ^1H NMR of PEI-LA and measured MTX concentration in MTX-PEI-LA. Thus, a molecular weight of 48.8 in PEI-LA and a molecular weight of 60.5 in MTX-PEI-LA contains one N, respectively. Based on the defined ratio of N/P, the weight of PEI-LA and MTX-PEI-LA required to complex a certain amount of miR-124 could be calculated. According to the weight percentages of PEI-LA and MTX-PEI-LA in the compositions of PHMs and M-PHMs, the corresponding weights of M-PHMs and PHMs required for a certain N/P ratio were calculated. As shown in Figure 2D, PHMs could successfully condense miR-124 with an N/P ratio of

12. When the N/P ratio was 16 or greater, M-PHMs could also completely condense miR-124 (Figure 2E). The MTX-PEI-LA or PEI-LA with a positive charge density in M-PHMs or PHMs is capable of having strong electrostatic interaction with the negatively charged miR-124. The size, zeta potential and PDI of the PHMs/miR-124 complexes (N/P=12) or M-PHMs/miR-124 complexes (N/P=16) were listed in Table S2. The size, zeta potential and PDI of PHMs/miR-124 were 112.7 ± 3.9 nm, 4.77 ± 1.85 mV, and 0.202 ± 0.001 (n=3). The size, zeta potential and PDI of M-PHMs/miR-124 were 116.6 ± 1.1 nm, -4.66 ± 0.20 mV, and 0.217 ± 0.008 (n=3), respectively. M-PHMs/miR-124 complexes had a smaller particle size than M-PHMs. This may be due to a more compact and stable structure of M-PHMs/miR-124 complexes after loaded with miR-124 by electrostatic interaction.

In vitro FAM-miR-124 release profile of M-PHMs/FAM-miR-124

In the FAM-miR-124 release profile (Figure S4), we found that M-PHMs had a slow and controlled release of FAM-miR-124 in phosphate buffer saline (PBS, pH=7.4). The cumulative release of FAM-miR-124 loaded in M-PHMs/FAM-miR-124 complexes was less than 25% within 48 h. In the first 2 h, the FAM-miR-124 in M-PHMs/FAM-miR-124 complexes had a rapid release and the cumulative

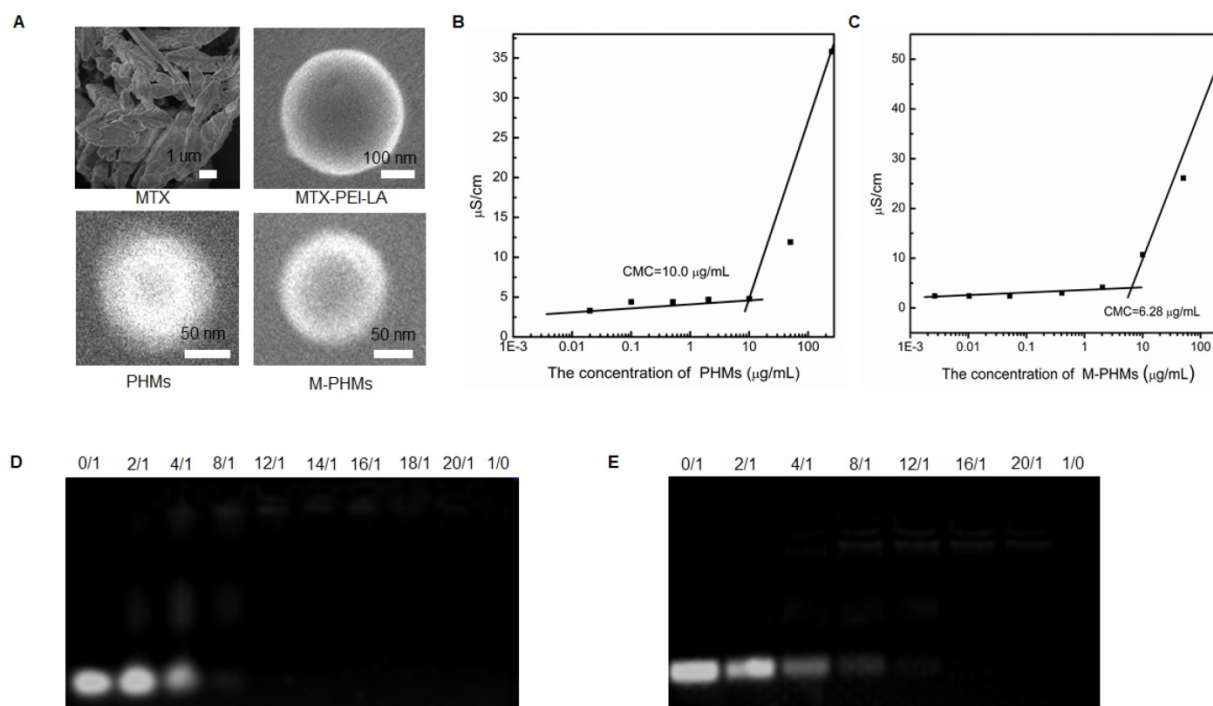


Figure 2. Characterization of PHMs and M-PHMs and their ability to complex miR-124. (A) The morphology of MTX, MTX-PEI-LA, PHMs, M-PHMs was obtained by field emission scanning electron microscopy (FESEM). The critical micelle concentration (CMC) of PHMs (B) and M-PHMs (C) was then obtained by measuring conductivity. The ability of PHMs (D), M-PHMs (E) to complex miR-124 was investigated by agarose gel electrophoresis. Nitrogen to phosphate ratios (N/P) of PHMs or M-PHMs to miR-124 varied from 0/1 to 20/1. N/P of 0/1 referred to the unencapsulated free miR-124. N/P of 1/0 referred to the vectors without miR-124.

release was up to 10%. This might be caused by the FAM-miR-124 adsorbed on the outer surface of the M-PHMs. At 10 h, the release of FAM-miR-124 reached a maximum. A strong interaction of FAM-miR-124 with the cationic carrier in M-PHMs may play an important role in the slow release of FAM-miR-124. The results also indicated high stability of the M-PHMs/FAM-miR-124 complexes in PBS. We also studied the release of MTX in M-PHMs. Consistent with a previous study, no free MTX was detected within 72 h [55, 67]. Since MTX was conjugated to the PEI-LA with a stable amide bond, MTX was not released in the PBS release medium at pH=7.4.

FR-mediated cell uptake of M-PHMs/Cy3-miR-124 in lipopolysaccharide (LPS)-induced RAW 264.7 cells

The murine macrophage cell line RAW 264.7 was induced by LPS (1 $\mu\text{g}/\text{mL}$) to obtain activated macrophage-like cells overexpressing FR β *in vitro* [45]. Cellular uptake mediated by the FR was first investigated and quantified by flow cytometry and further visualized by confocal microscopy (Figure 3). MTX-PEI-LA, RNAiMAX, M-PHMs, and PHMs were loaded with Cy3-miR-124 with red fluorescence. RNAiMAX was commercially available and set as a positive control for miR-124 delivery *in vitro*. According to the quantitative flow cytometric analysis, the cellular uptake intensity of M-PHMs/Cy3-miR-124 and MTX-PEI-LA/Cy3-miR-124 was depending on the activation status of macrophages. A much higher mean fluorescence intensity was found in M-PHMs/Cy3-miR-124 and MTX-PEI-LA/Cy3-miR-124 treated group compared with PHMs/Cy3-miR-124 without MTX conjugated in LPS-induced RAW 264.7 cells. The mean fluorescence intensity of LPS-induced RAW 264.7 cells treated with M-PHMs/Cy3-miR-124 was as strong as those treated with RNAiMAX/Cy3-miR-124. Simultaneously, the mean fluorescence intensity could be gradually decreased in activated macrophages pre-incubated with increasing FA concentrations (0.01 mM, 0.1 mM, 1 mM). MTX-PEI-LA/Cy3-miR-124 had a higher cellular uptake in LPS-induced RAW 264.7 cells than M-PHMs/Cy3-miR-124. This may be related to its higher positive charge. However, there was almost no significant difference in cellular uptake of M-PHMs/Cy3-miR-124 and MTX-PEI-LA/Cy3-miR-124 compared with PHMs/Cy3-miR-124 in non-activated macrophages (Figure 3A). Meanwhile, the mean fluorescence intensity of the cells treated with MTX-PEI-LA/Cy3-miR-124 and M-PHMs/Cy3-miR-124 was both low in RAW 264.7 cells without LPS induction. The pre-incubation of FA had no effect on

the cellular uptake of M-PHMs/Cy3-miR-124 in RAW 264.7 cells without LPS induction. The mean fluorescence intensity of RAW 264.7 cells treated with RNAiMAX/Cy3-miR-124 or PHMs/Cy3-miR-124, with or without LPS induction, was almost the same. The same results were observed in the confocal results. As was shown in Figure 3C-D, PHMs/Cy3-miR-124, MTX-PEI-LA/Cy3-miR-124, and M-PHMs/Cy3-miR-124 had lower uptake and lower red fluorescence intensity in non-activated macrophages. However, the red fluorescence intensity in the cytoplasm of activated macrophages treated with MTX-PEI-LA/Cy3-miR-124 or M-PHMs/Cy3-miR-124 was markedly stronger than those of cells treated with naked Cy3-miR-124 or PHMs/Cy3-miR-124. Furthermore, the fluorescence intensity of cells treated with M-PHMs/Cy3-miR-124 was significantly reduced and almost undetectable in cells pre-incubated with free FA (1 mM). Meanwhile, the red fluorescence intensity in non-activated macrophages treated with M-PHMs/Cy3-miR-124 was almost undetectable and had no significant change with preincubation with free FA (1 mM). These results demonstrated that the cellular uptake of M-PHMs/Cy3-miR-124 could be greatly increased in the activated macrophages and be inhibited by adding free FA. M-PHMs/Cy3-miR-124 entered FR-highly expressed macrophages mainly by FR-mediated endocytosis and had a promising FR targeting ability.

Endosome escape of M-PHMs/FAM-miR-124 in LPS-induced RAW 264.7 cells

The fluorescence-labeled complexes were efficiently taken up by RAW 264.7 macrophages with LPS activation. However, the drug release of M-PHMs/FAM-miR-124 at the subcellular level still remained unclear. Thus, another fluorescent reagent -Lyso Tracker™ Red DND-99 was used to label endosomes and investigate whether FAM-miR-124 could escape from the endosome and be released into the cytoplasm. As shown in Figure 4, the cellular uptake of M-PHMs/FAM-miR-124 was increased as the incubation time increased and the green fluorescence intensity reached the maximum value at 4 h. The green and red signals started to overlap at 1 h, indicating that M-PHMs/FAM-miR-124 began to be internalized into endosomes. At 2 h, the overlap of green and red signals started to increase. At 4 h, the overlap of green and red signals (orange color) reached a maximum, implying that FAM-miR-124 was all located in the endosome. At 6 h, the green signal was clearly isolated from the red signal, indicating that FAM-miR-124 had escaped from the endosome and was successfully released into the

cytosol. The endosome rupture may be due to the proton sponge effect of PEI in M-PHMs [60, 61]. All in all, miR-124 in M-PHMs/miR-124 could be efficiently internalized into the cells with high FR expression and successfully released into the cytoplasm.

Inhibition of nuclear factor of activated T cells

cytoplasmic I (NFATc1) expression and cell cytotoxicity of M-PHMs/miR-124

NFATc1 is the key factor for osteoclast differentiation and is induced by receptor activator of nuclear factor- κ B (NF- κ B) ligand (RANKL) [69, 70]. miR-124 has been reported to directly target NFATc1

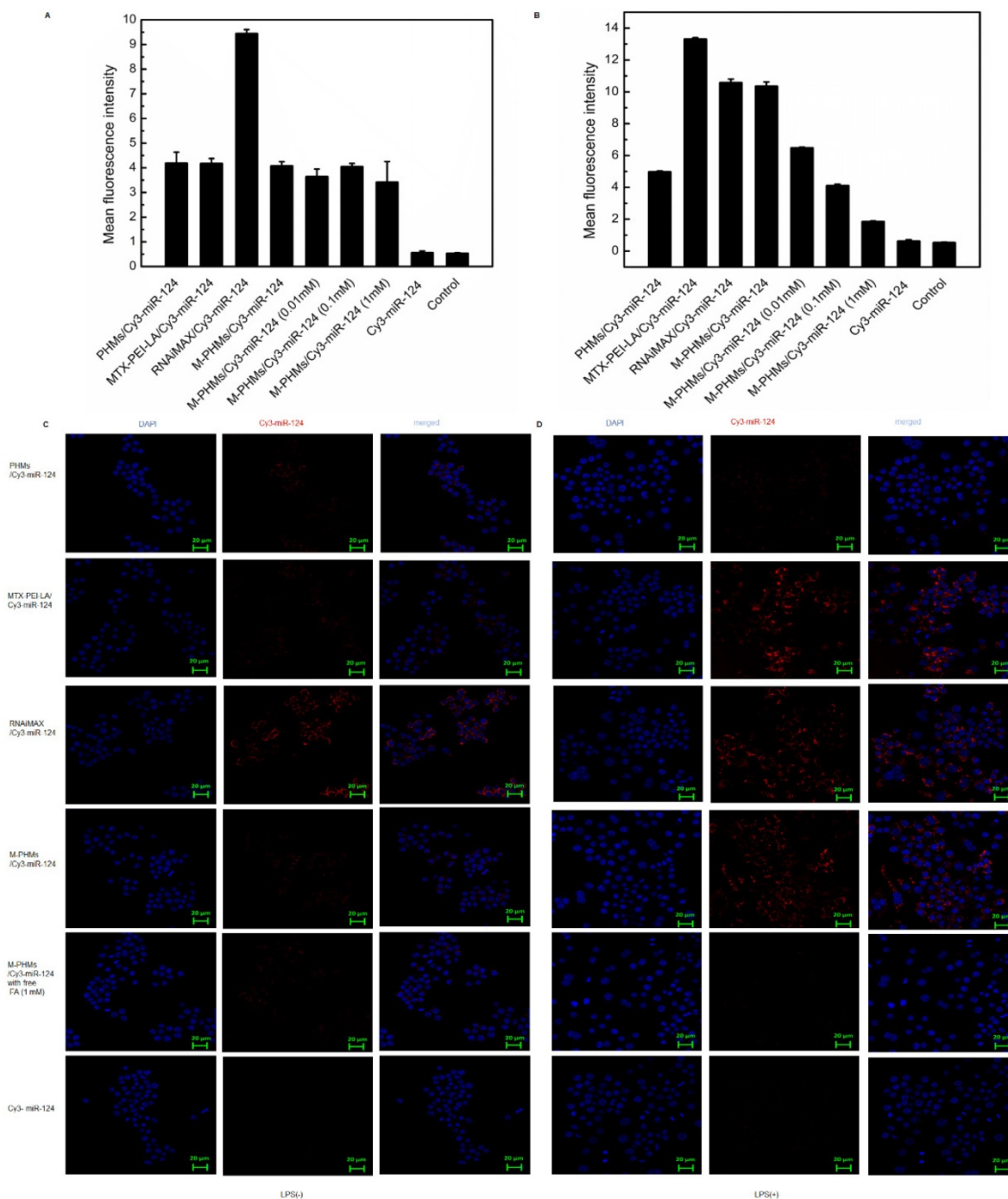


Figure 3. Cellular uptake of M-PHMs/Cy3-miR-124 *in vitro*. The RAW 264.7 cells were either activated by lipopolysaccharide (LPS) (+) or not (-). Flow cytometry was first used for quantitative analysis cell uptake of M-PHMs/Cy3-miR-124. RAW 264.7 cells activated by LPS (-) (A) or LPS (+) (B) were incubated with PHMs/Cy3-miR-124, MTX-PEI-LA/Cy3-miR-124, RNAiMAX/Cy3-miR-124, M-PHMs/Cy3-miR-124, or Cy3-miR-124 for 4 h at 37 °C. Free folic acid (FA) at increasing concentrations (0.01 mM, 0.1 mM, 1 mM) was added 1 h before M-PHMs/Cy3-miR-124 (100 nM) was added to the cells. RNAiMAX was commercially available and set as a positive control for miR-124 delivery. The values were mean \pm SEM (n = 3). Confocal micrographs of RAW 264.7 cells with LPS (-) (C) and LPS (+) (D) were then obtained after being incubated with MTX-PEI-LA/Cy3-miR-124, RNAiMAX/Cy3-miR-124, M-PHMs/Cy3-miR-124, and PHMs/Cy3-miR-124 for 4 h at 37 °C. Free FA was also added 1 h before the addition of M-PHMs/Cy3-miR-124 (100 nM) to the cells. Green Bar in the images was 20 μ m.

mRNAs, reduce NFATc1 expression levels, suppress the differentiation of osteoclast differentiation, and finally inhibit the progression of RA [27]. Therefore, the gene silencing efficiency of miR-124 can be assessed by measuring the expression level of NFATc1. As shown in **Figure S5**, RAW 264.7 cells stimulated with RANKL and treated with M-PHMs/miR-124 and MTX-PEI-LA/miR-124 had reduced NFATc1 expression levels compared with those treated with PHMs/miR-24, RNAiMAX/miR-124, or M-PHMs/miR-124 negative control (M-PHMs/miR-124 NC). M-PHMs/miR-124 NC referred to M-PHMs loaded with negative control miR-124. The results demonstrated that miR-124 delivered by M-PHMs and MTX-PEI-LA had been efficiently transfected into the cells and suppressed the expression of NFATc1. RAW 264.7 cells induced by LPS were then adopted to measure the cytotoxicity of the MTX conjugates through methyl thiazolyl tetrazolium (MTT) test. As shown in **Figure S6**, no cytotoxicity was observed for miR-124 in LPS-induced RAW 264.7 cells. Free MTX, MTX-PEI-LA, M-PHMs, M-PHMs/miR-124 NC, MTX-PEI-LA/miR-124, and

M-PHMs/miR-124 (MTX=0.29 $\mu\text{g}/\text{mL}$, miR-124=50 nM) had similar cytotoxicity after 48 h. Surprisingly, MTX-PEI-LA, MTX-PEI-LA/miR-124, and M-PHMs/miR-124 had a little stronger cytotoxicity than free MTX. This might be caused by the enhanced cellular uptake of MTX-PEI-LA compared with free MTX [55]. However, RNAiMAX/miR-124 showed the strongest cytotoxicity to the LPS-induced RAW 264.7 cells. The high cytotoxicity was caused by the carrier RNAiMAX. The results suggested that although RNAiMAX had a high transfection efficiency (**Figure 3**), the carrier cytotoxicity cannot be ignored (**Figure S6**). Compared to RNAiMAX, M-PHMs exhibited lower carrier toxicity when complexed with the same amount of miR-124. Although MTX-PEI-LA/miR-124 showed a higher cellular uptake, transfection efficiency, and cytotoxicity compared with M-PHMs/miR-124 *in vitro* (**Figure 3**, **Figure S5** and **Figure S6**), MTX-PEI-LA was still unsuitable for *in vivo* use due to its higher positive charge, BSA precipitation rate and potential instability in the blood (**Figure S3**). Therefore, RNAiMAX and MTX-PEI-LA were not included in the *in vivo* therapeutic studies.

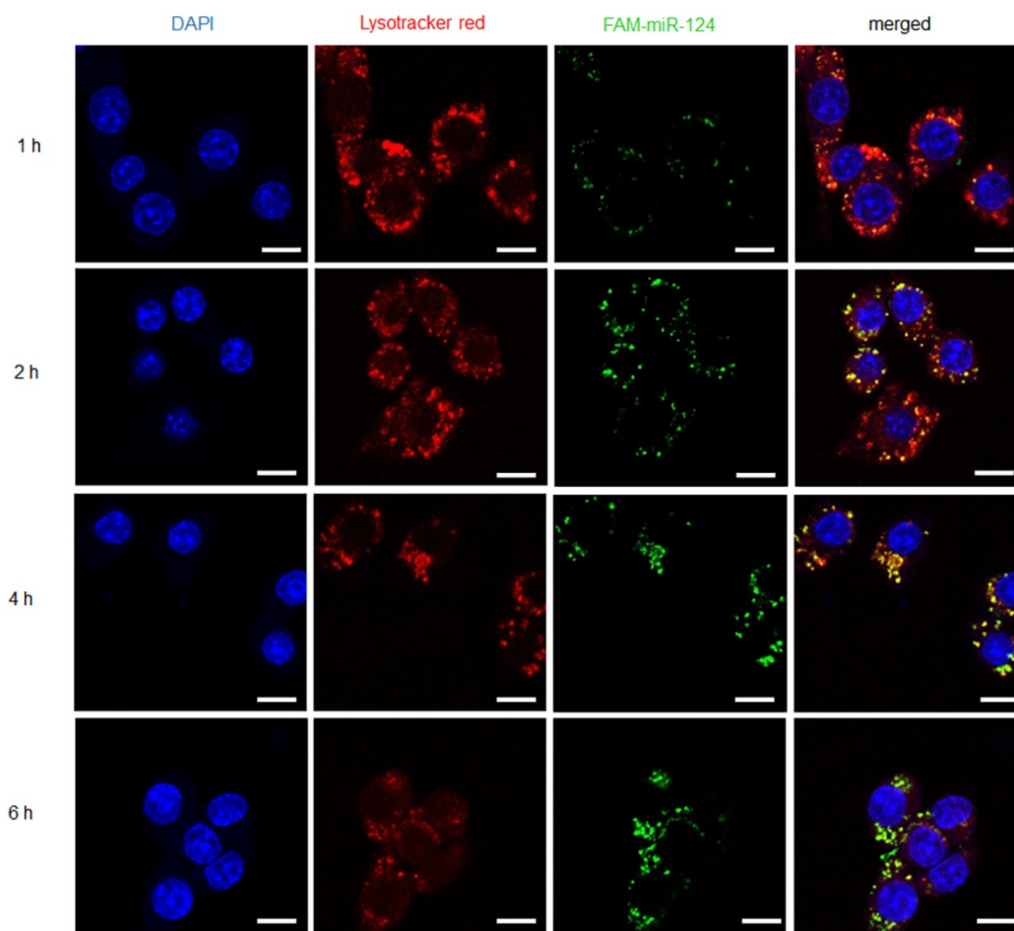


Figure 4. Internalization and endosome escape of M-PHMs/FAM-miR-124 complexes in activated RAW 264.7 cells. Internalization process and escape of M-PHMs loaded with FAM-miR-124 (green) from endosomes (red) of activated macrophages was visualized by confocal laser scanning microscopy (CLSM) at 1, 2, 4, and 6 h. The scale bar in the images was 10 μm .

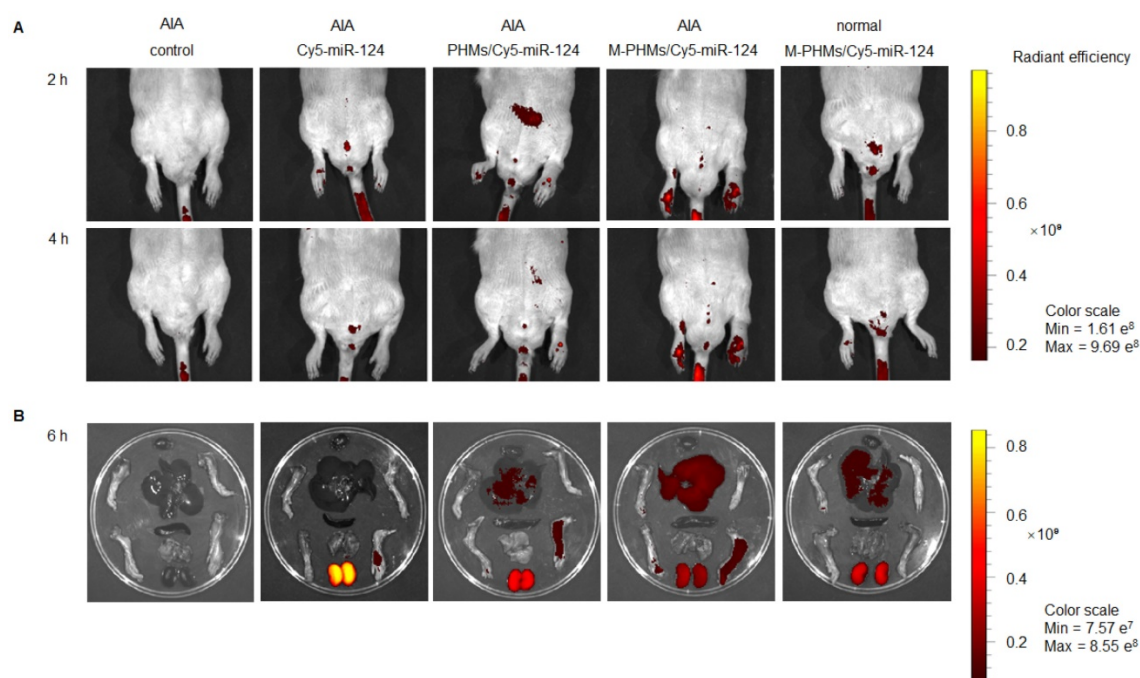


Figure 5. Bio-distribution of M-PHMs/miR-124 *in vivo*. (A) Real-time fluorescence imaging of AIA rat injected with the naked Cy5-miR-124, PHMs/Cy5-miR-124 or M-PHMs/Cy5-miR-124 (Cy5-miR-124=2 nmol) via the tail vein was obtained at 2 and 4 h after administration. (B) Ex vivo imaging of the paws and organs excised from AIA and normal rats was imaged at 6 h after injection. The AIA rat injected with saline and the normal rat injected with M-PHMs/Cy5-miR-124 were set as the blank and negative control, respectively. Images were obtained by IVIS[®] *In Vivo* Imaging System with an optimized parameter (excitation, 640 nm; emission, 700 nm).

Hemolytic analysis of M-PHMs/miR-124 and PHMs/miR-124

To investigate the blood biocompatibility of the complexes for systemic delivery *in vivo*, a hemolysis test was carried out. As shown in **Figure S7A-C**, no obvious erythrocyte hemolysis was observed in the M-PHMs/miR-124, PHMs/miR-124, and MTX groups. The hemolytic ratios of MTX, M-PHMs/miR-124, and PHMs/miR-124 were both below 2.5%, suggesting good biocompatibility and safety when administered intravenously (**Figure S7D**). Good biocompatibility may depend largely on the PEG layer in the particles [68]. Besides, M-PHMs/miR-124 complexes had a lower hemolytic activity compared with PHMs/miR-124. This may be related to the lower positive charge on the surface of M-PHMs/miR-124 complexes (**Table S2**).

In vivo biodistribution of M-PHMs/miR-124 in inflamed joints

Although the M-PHMs/miR-124 could be efficiently taken up by the activated macrophages with high FR expression *in vitro*, efficient co-delivery of microRNA and MTX to the activated macrophages in inflamed joints was a prerequisite for successful therapy in RA. Thus, the fluorescence intensity of the complexes in AIA rats was investigated and quantified (**Figure 5** and **Figure S8**). As shown in **Figure 5**, the naked Cy5-miR-124 was quickly cleared by the kidney *in vivo*. The fluorescence intensity

percentage of naked Cy5-miR-124 in the kidney was 81.9%, while the fluorescence intensity percentage in liver and joints is only 10.5% and 5.6% (**Figure S8**). The AIA rat injected with M-PHMs/Cy5-miR-124 complexes exhibited the highest fluorescence intensity in inflammatory joints (**Figure 5**). The percentage of fluorescence intensity at the inflammatory joint site in the M-PHMs/Cy5-miR-124 treatment group was 1.3-fold and 3-fold higher than that of the PHMs/Cy5-miR-124 complex and the naked Cy5-miR-124 (**Figure S8**). Compared with PHMs/Cy5-miR-124 group, M-PHMs/Cy5-miR-124 group showed a significant fluorescence intensity percentage increase in the liver (54.4% vs. 34.8%), while there was a reduction in the kidneys (24.1% vs. 46.7%) (**Figure S8**). The positive charge on the PHMs/Cy5-miR-124 complexes (**Table S2**) may result in the rapid clearance of PHMs/Cy5-miR-124 *in vivo*. PHMs/Cy5-miR-124 group was also observed a much higher distribution in the inflamed joints than the naked Cy5-miR-124 group. This may be due to the passive targeting of nanosized particles through enhanced permeability and retention effect (EPR) in inflammation sites as previous studies indicated [29, 71, 72]. The studies confirmed that M-PHMs/Cy5-miR-124 could efficiently target and specifically deliver Cy5-miR-124 to the inflamed joints. The previous study has shown that FR-targeted nanocarriers are more likely to accumulate at sites of inflammation than tumors that express high FR [72].

Therefore, M-PHMs/Cy5-miR-124 targeting activated macrophages may have a good prospect in RA therapy [73].

Therapeutic efficacy of M-PHMs/miR-124 in AIA rat model

Bone changes assessed are more severe in AIA rats than in collagen-induced arthritis models. The hallmark of the AIA model is reliable disease initiation and progression, and it is easy to measure articular inflammation and significant bone destruction [74, 75]. Thus, to evaluate the synergy of MTX and miR-124, AIA model was established. Anti-inflammatory effect on AIA rats was evaluated by the measurement of the hind paws thickness, scores of the fore and hind paws, photographs of hind paws (**Figure 6A-C** and **Figure S9**). Bone changes in joints were assessed by X-ray photograph (**Figure 6D**). As shown in **Figure 6A-B**, left hind paw thickness and arthritis score of saline and free MTX treated animals were gradually increased indicating disease progression, while this progression was decreased in animals treated with M-PHMs/miR-124 NC, PHMs/miR-124 and M-PHMs/miR-124. Animals treated with M-PHMs/miR-124 were found to be a highly significant symptom remission compared with MTX (** $P < 0.001$), M-PHMs/miR-124 NC (** $P < 0.01$) and PHMs/miR-124 (* $P < 0.05$) in paw thickness, swelling, and erythema score. AIA rats treated with M-PHMs/miR-124 NC and PHMs/miR-124 were also found to have reduced paw thickness, swelling and erythema score compared with saline and MTX group. In addition, as shown in **Figure S9**, only the right ankle thickness of AIA rat treated with saline was greatly increased. This indicates that the drug-administered groups can inhibit the disease progression of the contralateral joint. Similar results were also observed from the photographs of hind paws (**Figure 6C**). Compared with the clearly visible of joints by X-ray photograph with uniform and integrity in normal rats and M-PHMs/miR-124 treated groups, physiological saline and free MTX treated animals had a vague shadow, incompleteness of bone structure and an obvious bone loss and damage as the red arrow indicated (**Figure 6D**). The integrity of articular cartilage in the PHMs/miR-124 group was found to be superior to that of the M-PHMs/miR-124 NC, MTX and saline groups as the red arrows indicated. Both M-PHMs/miR-124 and PHMs/miR-124 group had obvious bone protection. This suggested strong bone protection of miR-124 as previous studies reported [27].

As shown in **Figure 5** and **Figure S8**, M-PHMs/Cy5-miR124 complexes injected to the AIA rat showed a high fluorescence intensity in the liver

compared to other groups. Therefore, histological analysis of liver excised from groups treated with different formulations was investigated to justify whether MTX in M-PHMs/miR-124 can cause hepatotoxicity. As shown in **Figure S10**, there was no obvious hepatotoxicity in the groups treated with saline, M-PHMs/miR-124, M-PHMs/miR-124 NC, PHMs/miR-124, and MTX compared with the normal group. Actually, the dose of the MTX (38 $\mu\text{g}/\text{kg}$) via tail vein injection was low and could not cause toxicity even a high accumulation of M-PHMs/miR-124 in the liver. Body weight of the AIA rats was also measured to confirm whether the micelles had systemic toxicity upon the drug administration. The body weight of AIA rats treated with different formulations was found to be steadily increased and there was no significant difference (**Figure S11**). The formulations had no obvious injection toxicity.

The serum concentration of pro-inflammatory cytokines in AIA rats

Cytokines play a central role in the progression of arthritic diseases [2]. Enhanced levels of pro-inflammatory crucial cytokines such as TNF- α , IL-1 β , IL-17, IL-18, IL-6, IL-12 often result in chronic inflammatory responses and destruction of joints [76, 77]. Therefore, the serum expression levels of crucial pro-inflammatory cytokines in AIA rats treated with different formulations were determined for further evaluation of the progression of the arthritis disease. As shown in **Figure 7**, TNF- α , IL-1 β , IL-17, IL-18, IL-6, IL-12 expression levels were significantly inhibited in the serum of M-PHMs/miR-124 treated group. Compared with M-PHMs/miR-124 NC and PHMs/miR-124 groups, M-PHMs/miR-124 treated group had the least concentration of TNF- α (** $P < 0.01$, **Figure 7A**), IL-1 β (* $P < 0.05$, **Figure 7B**) and IL-17 (** $P < 0.01$, **Figure 7C**). This indicated a synergy of MTX and miR-124 in reducing the expression of TNF- α , IL-1 β , and IL-17. A reduced serum levels of TNF- α (** $P < 0.01$), IL-17 (* $P < 0.05$), IL-18 (* $P < 0.05$), IL-6 (* $P < 0.05$, **Figure 7E**), IL-12 (* $P < 0.05$) were found in M-PHMs/miR-124 NC group (MTX conjugates alone). AIA rats treated with PHMs/miR-124 (miR-124 alone) were also found to have a reduced TNF- α (* $P < 0.05$), IL-6 (* $P < 0.05$), IL-18 (** $P < 0.01$), IL-12 (** $P < 0.01$). Compared with PHMs/miR-124 treatment group, M-PHMs/miR-124 NC group showed a stronger inhibition effect of TNF- α , IL-1 β , IL-17, and IL-6 expression which were often measured to confirm the efficacy of MTX as previous studies indicated [35, 78]. While in AIA rats treated with PHMs/miR-124, the serum levels of IL-18 (**Figure 7D**) and IL-12 (**Figure 7F**) was lower than

M-PHMs/miR-124 NC group. There may be a close relation between miR-124, IL-12, and IL-18. In conclusion, the combination of MTX and miR-124 suggested a synergistic inhibition of cytokines expression.

Histopathologic analysis of joints in AIA rats

The histopathologic analysis was applied to observe the pathological changes in joints of AIA rats treated with different formulations (Figure 8). The ankle joint sections stained with hematoxylin-eosin (HE), toluidine blue (TB), tartrate-resistant acid phosphatase (TRAP) were conducted to investigate synovial hyperplasia, cartilage and bone erosion, and osteoclast generation in animals treated with different formulations. Black arrows indicated severe synovial hyperplasia and cellular infiltrates (Figure 8A). The red arrows indicated severe destruction and incompleteness of articular cartilage (Figure 8B). The blue arrows referred to the generation of osteoclasts (Figure 8C). Stained ankle joints of AIA rats treated with saline and free MTX revealed the most severe synovial hyperplasia, degradation and destruction of articular cartilage tissue, and contained the most osteoclast clusters. Synovial hyperplasia was

somewhat less extensive in animal groups treated with M-PHMs/miR-124 NC and PHMs/miR-124, as shown in Figure 8A. Animals treated with M-PHMs/miR-124 complexes showed the mildest histopathology, with clear and smooth cartilage, fewer and lighter synovial hyperplasia and less infiltration by inflammatory cells compared with other groups in Figure 8A. Similar results were obtained by analyzing ankle joint sections stained with TB, which indicated the degree of cartilage destruction (Figure 8B). The osteoblasts could be colored to blue by TB. Animals treated with M-PHMs/miR-124 complexes had cartilage as intact as normal rats. Compared to the M-PHMs/miR-124 NC, cartilage was less damaged in animals treated with PHMs/miR-124. The results were consistent with the results of Figure 6D and further demonstrated the cartilage protection of miR-124. However, M-PHMs/miR-124 NC also showed weak cartilage protection. Due to the pro-inflammatory cytokines often resulted in joint and cartilage destruction, the weak cartilage protection may be caused by the reduced pro-inflammatory cytokines of M-PHMs/miR-124 NC (Figure 7).

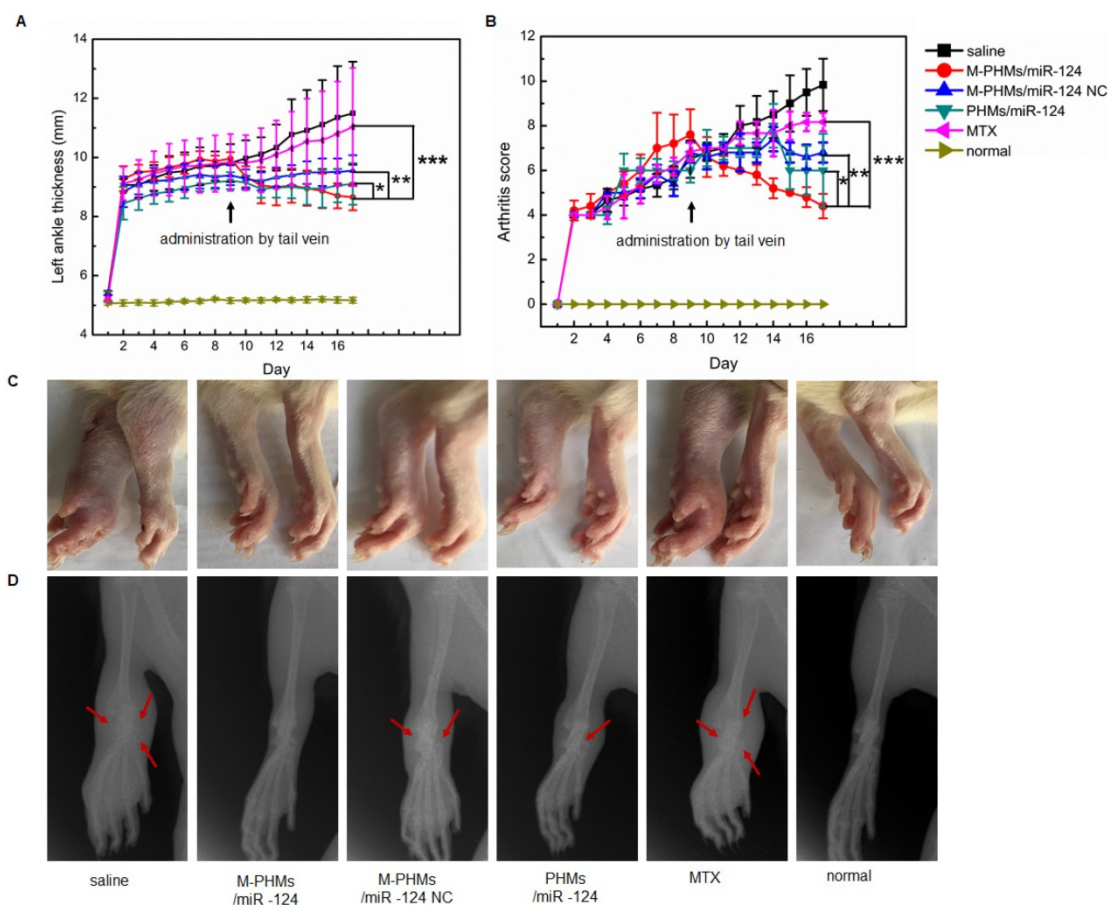


Figure 6. Therapeutic efficacy of M-PHMs/miR-124 *in vivo*. Left ankle thickness (A) and clinical score of AIA rats (B) treated with various drug formulations were obtained (*P < 0.05, **P < 0.01, ***P < 0.001, PHMs/miR-124, PHMs/miR-124 NC, and MTX separately compared with M-PHMs/miR-124). (C) Photographs of hind paws and representative X-ray of the left ankle (D) from AIA rats treated with various drug formulations. Rats without AIA were set as normal group. Values are mean \pm SEM (n=6).

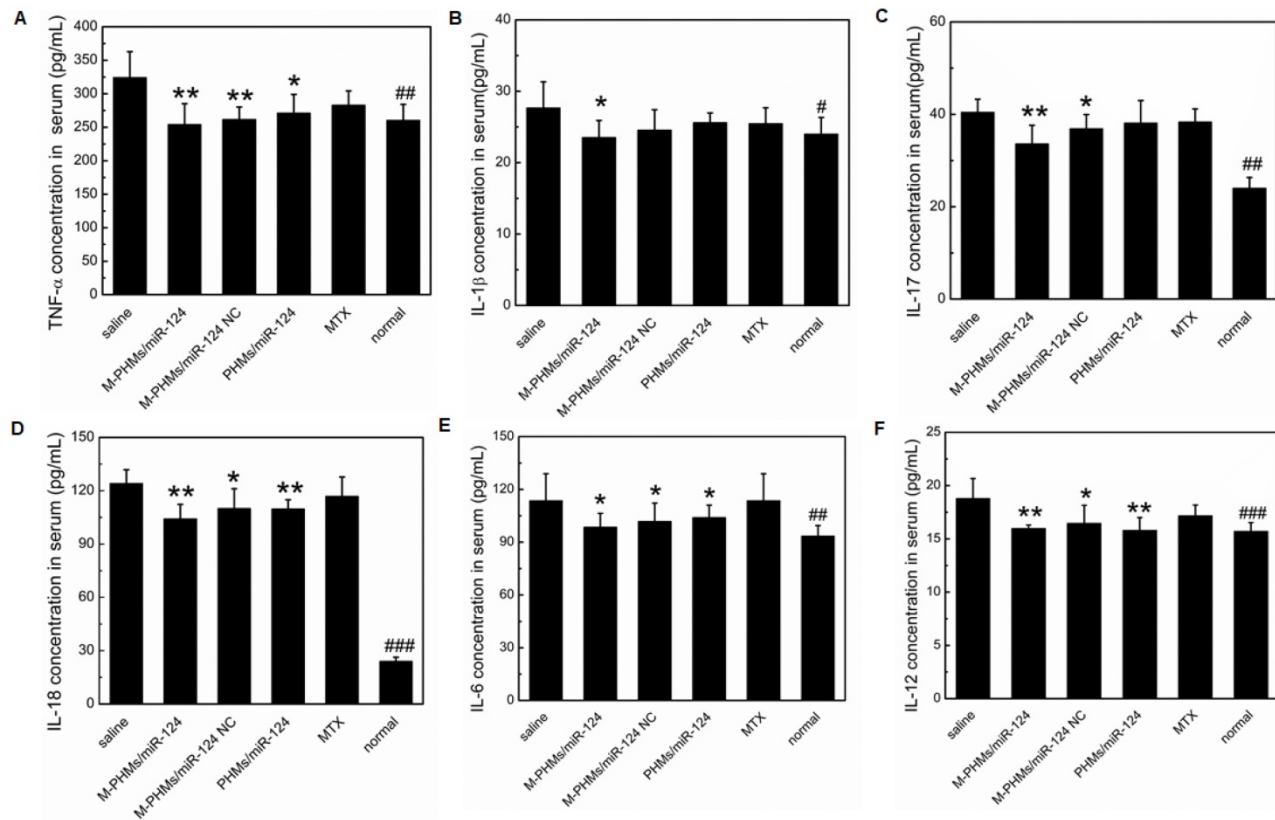


Figure 7. The serum concentration of pro-inflammatory cytokines. Serum levels of the pro-inflammatory cytokines TNF- α (A), IL-1 β (B), IL-17 (C), IL-18 (D), IL-6 (E) and IL-12 (F) were measured in AIA rats treated with different formulations (n=6, mean \pm SEM, *P < 0.05, **P < 0.01, ***P < 0.001, M-PHMs/miR-124, M-PHMs/miR-124 NC, PHMs/miR-124, and MTX treated AIA rats separately compared with AIA rats treated with saline group, #P < 0.05, ##P < 0.01, ###P < 0.001, normal rat group compared with AIA rats treated with saline).

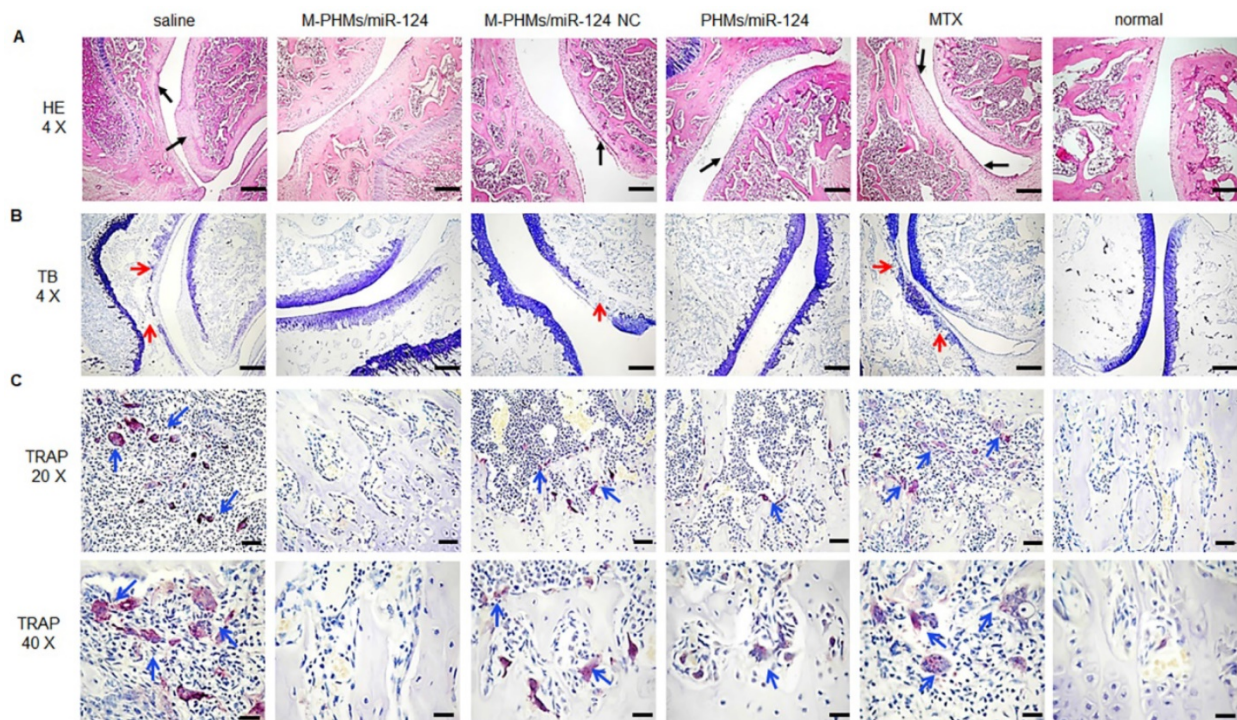


Figure 8. Histopathological examination of AIA rat joints. Hematoxylin-eosin (HE), toluidine blue (TB) and tartrate-resistant acid phosphatase (TRAP) staining analyses were performed on joints section from AIA rats treated with saline, M-PHMs/miR-124, M-PHMs/miR-124 NC, PHMs/miR-124 and MTX. Histopathological examination of normal rat group was set as a blank control. (A) HE staining was applied to study synovial hyperplasia. Black arrows indicated severe synovial hyperplasia. (B) TB staining of joints was conducted to analyze the integrity of articular cartilage. The red arrows indicated severe destruction and incompleteness of articular cartilage. (C) TRAP staining was used to study the number of osteoclasts. The blue arrows referred to the clusters of osteoclasts. The scale bar in HE (4 X, A) and TB (4 X, B) was 500 μ m. The scale bars in TRAP (20 X and 40 X) were 100 μ m and 50 μ m, respectively.

miR-124 was previously reported to inhibit the progression of AIA rats by reducing the osteoclast differentiation [25, 27, 28]. Thus, TRAP staining was further performed to investigate the number of osteoclasts in joints of AIA rats. Purple stain area referred to the osteoclasts clusters as blue arrows indicated (**Figure 8C**) and the TRAP (+) cells number and TRAP (+) area were further quantified by using Image pro-plus 6.0 (**Figure S12**). As shown in **Figure 8C** and **Figure S12**, saline and free MTX group had a large number of osteoclasts (13.6 folds and 10.8 folds than normal group per cm^3) generation and much larger purple stain area (24.4 folds and 16.1 folds purple area than normal group). The increased osteoclasts may be a major cause for severe cartilage destruction of the two groups. M-PHMs/miR-124 complexes treated AIA rats had the least of TRAP (+) cells number (**P < 0.001) and the smallest TRAP (+) area (**P < 0.01) compared with M-PHMs/miR-124 NC, PHMs/miR-124, MTX and saline groups. The TRAP (+) cells number of M-PHMs/miR-124 NC, PHMs/miR-124, MTX and saline groups was 3.87 folds, 3.00 folds, 4.12 folds, and 5.12 folds that of M-PHMs/miR-124. The TRAP (+) area in M-PHMs/miR-124 NC, PHMs/miR-124, MTX and saline groups was 3.89 folds, 2.90 folds, 7.65 folds, and 11.57 folds that of M-PHMs/miR-124. The results of TRAP staining further exhibited that the miR-124 in M-PHMs/miR-124 was most efficiently delivered to the macrophages in inflamed joint, reduced the number of osteoclasts, and ultimately prevented the bone destruction.

Despite the long clinical history of MTX in RA, the exact mechanism of low-dose MTX anti-inflammatory action is still not fully understood. The enhancement of adenosine signaling has been strongly supported by animal model studies and some of which even have been confirmed in humans [16]. As shown previously, MTX or MTX conjugates therapy can be assessed by measuring the thickness of the swollen joints, clinic score, and proinflammatory cytokines levels and histopathological analysis of joints [34, 35, 47]. miR-124 has a direct bone protective effect in the context of RA by suppressing the differentiation of human osteoclasts and has anti-inflammatory activity in RA by inhibiting proinflammatory cytokines levels [26, 27]. To assess the bone protection of M-PHMs/miR-124, we performed an X-ray imaging, TB and TRAP staining analysis of joints section in AIA rats. Therefore, from the results of **Figure 6**, **Figure 7**, **Figure 8** and **Figure S12**, it could be concluded that M-PHMs/miR-124 achieved a combination therapy of MTX and miR-124 in AIA rats.

Compared with free MTX, a mild anti-inflammatory effect was observed in AIA rats treated with M-PHMs/miR-124 NC (MTX conjugates) (**Figure 6**, **Figure 7**, **Figure 8** and **Figure S12**). This may be due to the good stability and targeting efficiency of MTX conjugates, which finally improved the amount of MTX conjugates in the targeted macrophages [42, 46]. Since MTX was conjugated to the PEI-LA with a stable amide bond, as demonstrated in the previous study, the MTX conjugates may work primarily in two ways: 1) MTX conjugates directly bind to the target protein and obtain the therapeutic effects [53, 79, 80]; 2) MTX conjugates may release MTX through cytoplasmic protease-mediated peptide bond cleavage due to the presence of many types and functions of proteases in cells or lysosome [81-83]. Therefore, the release of free MTX may not be necessary to achieve the therapeutic efficacy of MTX conjugates. The MTX-PEI-LA conjugates in M-PHMs may be an active agent of RA treatment.

A moderate therapeutic efficiency was also observed by PHMs/miR-124 treated group. This might be due to the EPR effect of PHMs that promotes the accumulation of miR-124 in the joint and might also be associated with the therapeutic effects of free miR-124. However, as shown in **Figure 5** and **Figure S6**, compared with free miR-124, PHMs/miR-124 group had a higher accumulation of miR-124 (2.3 folds than free miR-124) in joint and much slower clearance rate. The greater miR-124 accumulation in joint may contribute to a good therapeutic effect of PHMs/miR-124. This may be explained by the passive targeting of the PHMs/miR-124 through the EPR effect of nanosized micelles [29, 84, 85].

Above all, based on the results of joint thickness, clinical score, X-ray photograph, serum concentration of pro-inflammatory cytokines and histological analysis of joints *in vivo* (**Figure 6**, **Figure 7** and **Figure 8**), we concluded that a synergy effect of M-PHMs/miR-124 may mainly depend on the MTX conjugates and miR-124 anti-inflammatory effect and miR-124 bone protection. The results implied that the M-PHMs/miR-124 complexes exhibited a greater effect compared with M-PHMs/miR-124 control and PHMs/miR-124. This might be due to the specific and efficient delivery of miR-124 and MTX conjugates to the activated macrophages in arthritis sites. The efficient therapy effect especially a direct bone protective effect *in vivo* may be explained by the MTX mediated folate receptor targeting and enhanced miR-124 delivery, resulting in the reduction of the osteoclasts generation and suppression of cartilage destruction. However, the specific and detailed therapy mechanism and the synergistic effect of

co-delivery of MTX and miR-124 still require further investigation.

Conclusion

In this work, two polymer components, MTX-PEI-LA, and mPEG-LA were synthesized and used to prepare the dual functional M-PHMs with miR-124 encapsulation by a simplified, tunable and smart approach. The M-PHMs/miR-124 complexes exhibited a strong FR β targeting ability on the activated macrophages, were internalized by FR-mediated endocytosis, and successfully escaped from the endosome, released miR-124 into the cytoplasm and then down-regulated the expression of NFATc1. Biodistribution and therapeutic activity in an AIA rat model demonstrated that M-PHMs/miR-124 could specifically target the inflamed joints and achieve an enhanced synergistic efficacy of MTX and miR-124 *in vivo*. In addition, we presented a new rational design for drug co-delivery. The bifunctional and efficient drug delivery system with a simple design could be applied to other disease therapy by changing the payload.

Abbreviations

RA: rheumatoid arthritis; DMARDs: disease-modifying antirheumatic drugs; MTX: methotrexate; miR-124: microRNA-124; AIA: adjuvant-induced arthritis; folate receptor beta FR β : folate receptor beta; SR: scavenger receptor; FA: folate acid; G5: generation 5 dendrimer; FR α : folate receptor aerfa; PEI: polyethyleneimine; DOX: doxorubicin; MTX-PEI-LA: MTX linked to polyethyleneimine with linoleic acid conjugated; M-PHMs: MTX-conjugated polymer hybrid micelles; mPEG-LA: linoleic acid-modified methyl polyethylene glycol; FT-IR: fourier-transform infrared; LC: linoleyl chloride; CDCl₃: deuterated chloroform; DMSO-d₆: deuterated dimethyl sulfoxide; D₂O: deuterated water; PDI: polydispersity index; BSA: bovine serum albumin; PHMs: polymer hybrid micelles; FESEM : field emission scanning electron microscopy; PEG: polyethylene glycol; CMC: critical micelle concentration; N/P: nitrogen to phosphate ratio; PBS: phosphate buffer solution; LPS: lipopolysaccharide; NFATc1: nuclear factor of activated T cells cytoplasmic 1; RANKL: receptor activator of nuclear factor- κ B (NF- κ B) ligand; M-PHMs/miR-124 NC: M-PHMs/miR-124 negative control; MTT: methyl thiazolyl tetrazolium; EPR: enhanced permeability and retention effect; H&E: hematoxylin and eosin; TB: toluidine blue; TRAP: tartrate-resistant acid phosphatase.

Supplementary Material

Supplementary experimental section, FT-IR spectra of the synthesized amphiphilic polymer, the wavelength scan of MTX-PEI-LA, size and zeta potential of M-PHMs with different ratios of MTX-PEI-LA, size and zeta potential of M-PHMs/miR-124, BSA adsorption assay, miR-124 release in M-PHMs/miR-124, Inhibition of NFATc1 expression, cell viability, hemolysis analysis, fluorescence intensity percentage in dissected organs and joints, right ankle thickness, histological analysis of the liver, body weight of AIA rats, quantitative analysis of TRAP (+) cells number and TRAP (+) area.
<http://www.thno.org/v09p5282s1.pdf>

Acknowledgments

The biodistribution and histopathologic analysis in this article were obtained with IVIS[®] spectrum system and with technical support from the Key Laboratory of Pathology and Biology Teaching of Ministry of Education and Basic Medical Experimental Teaching Center of Jilin University.

Competing Interests

The authors have declared that no competing interest exists.

References

- Smolen JS, Aletaha D, Barton A, Burmester GR, Emery P, Firestein GS, et al. Rheumatoid arthritis. *Nat Rev Dis Primers*. 2018; 4: 18001.
- Alam J, Jantan I, Bukhari SNA. Rheumatoid arthritis: Recent advances on its etiology, role of cytokines and pharmacotherapy. *Biomedicine*. 2017; 92: 615-33.
- Guo Q, Wang Y, Xu D, Nossent J, Pavlos NJ, Xu J. Rheumatoid arthritis: pathological mechanisms and modern pharmacologic therapies. *Bone Res*. 2018; 6: 15.
- Smolen JS, Landewe R, Bijlsma J, Burmester G, Chatzidionysiou K, Dougados M, et al. EULAR recommendations for the management of rheumatoid arthritis with synthetic and biological disease-modifying antirheumatic drugs: 2016 update. *Ann Rheum Dis*. 2017; 76: 960-77.
- Burmester GR, Pope JE. Novel treatment strategies in rheumatoid arthritis. *Lancet*. 2017; 389: 2338-48.
- Wang Q, Jiang H, Li Y, Chen W, Li H, Peng K, et al. Targeting NF- κ B signaling with polymeric hybrid micelles that co-deliver siRNA and dexamethasone for arthritis therapy. *Biomaterials*. 2017; 122: 10-22.
- Park JS, Yang HN, Jeon SY, Woo DG, Kim MS, Park KH. The use of anti-COX2 siRNA coated onto PLGA nanoparticles loading dexamethasone in the treatment of rheumatoid arthritis. *Biomaterials*. 2012; 33: 8600-12.
- Churov AV, Oleinik EK, Knip M. MicroRNAs in rheumatoid arthritis: altered expression and diagnostic potential. *Autoimmun Rev*. 2015; 14: 1029-37.
- Wittmann J, Jack HM. microRNAs in rheumatoid arthritis: midget RNAs with a giant impact. *Ann Rheum Dis*. 2011; 70 (Suppl 1): S92-6.
- Fleischmann R, Lin Y, St John G, van der Heijde D, Qiu C, Jose Gomez-Reino J, et al. Long-Term Safety with Sarilumab Plus Conventional Synthetic Disease-Modifying Antirheumatic Drugs (csDMARDs) and Sarilumab Monotherapy in Rheumatoid Arthritis (RA): An Integrated Analysis with 9,000 Patient-Years (Pt-Yrs) of Follow-up. *Arthritis Rheumatol*. 2018; 70 (Supplement 9): 2527.
- Takeuchi T, Tanaka Y, Soen S, Yamanaka H, Yoneda T, Tanaka S, et al. Effects of the anti-RANKL antibody denosumab on joint structural damage in patients with rheumatoid arthritis treated with conventional synthetic disease-modifying antirheumatic drugs (DESIRABLE study): a randomised, double-blind, placebo-controlled phase 3 trial. *Ann Rheum Dis*. 2019; [Epub ahead of print].
- Abbasi M, Mousavi MJ, Jamalzahi S, Alimohammadi R, Bezvan MH, Mohammadi H, et al. Strategies toward rheumatoid arthritis therapy; the old and the new. *J Cell Physiol*. 2019; 234: 10018-31.

13. Shinde CG, Venkatesh MP, Kumar TM, Shivakumar HG. Methotrexate: a gold standard for treatment of rheumatoid arthritis. *J Pain Palliat Care Pharmacother.* 2014; 28: 351-8.
14. Visser K, van der Heijde D. Optimal dosage and route of administration of methotrexate in rheumatoid arthritis: a systematic review of the literature. *Ann Rheum Dis.* 2009; 68: 1094-9.
15. Xu K, Cai YS, Lu SM, Li XL, Liu L, Li Z, et al. Autophagy induction contributes to the resistance to methotrexate treatment in rheumatoid arthritis fibroblast-like synovial cells through high mobility group box chromosomal protein 1. *Arthritis Res Ther.* 2015; 17: 374.
16. Brown PM, Pratt AG, Isaacs JD. Mechanism of action of methotrexate in rheumatoid arthritis, and the search for biomarkers. *Nat Rev Rheumatol.* 2016; 12: 731-42.
17. Schnabel A, Gross WL. Low-dose methotrexate in rheumatic diseases—efficacy, side effects, and risk factors for side effects. *Semin Arthritis Rheum.* 1994; 23: 310-27.
18. Subesinghe S, Scott IC. Key findings from studies of methotrexate tapering and withdrawal in rheumatoid arthritis. *Expert Rev Clin Pharmacol.* 2015; 8: 751-60.
19. van Vollenhoven RF, Geborek P, Forslind K, Albertsson K, Ernestam S, Petersson IF, et al. Conventional combination treatment versus biological treatment in methotrexate-refractory early rheumatoid arthritis: 2 year follow-up of the randomised, non-blinded, parallel-group Swefot trial. *Lancet.* 2012; 379: 1712-20.
20. Sun Y, Yao Y, Ding CZ. A combination of sinomenine and methotrexate reduces joint damage of collagen induced arthritis in rats by modulating osteoclast-related cytokines. *Int Immunopharmacol.* 2014; 18: 135-41.
21. Westhovens R, Taylor PC, Alten R, Pavlova D, Enriquez-Sosa F, Mazur M, et al. Filgotinib (GLPG0634/GS-6034), an oral JAK1 selective inhibitor, is effective in combination with methotrexate (MTX) in patients with active rheumatoid arthritis and insufficient response to MTX: results from a randomised, dose-finding study (DARWIN 1). *Ann Rheum Dis.* 2017; 76: 998-1008.
22. Hazlewood GS, Barnabe C, Tomlinson G, Marshall D, Devoe D, Bombardier C. Methotrexate monotherapy and methotrexate combination therapy with traditional and biologic disease modifying antirheumatic drugs for rheumatoid arthritis: abbreviated Cochrane systematic review and network meta-analysis. *BMJ.* 2016; 353: i1777.
23. Rupaimoole R, Slack FJ. MicroRNA therapeutics: towards a new era for the management of cancer and other diseases. *Nat Rev Drug Discov.* 2017; 16: 203-22.
24. Rupaimoole R, Han H-D, Lopez-Berestein G, Sood AK. MicroRNA therapeutics: principles, expectations, and challenges. *Chin J Cancer.* 2011; 30: 368-70.
25. Nakamachi Y, Saegusa J, Kawano S. MicroRNA-124: A promising therapeutic agent for various human diseases, including rheumatoid arthritis. *RNA Dis.* 2016; 3: e1252.
26. Sun Y, Li Q, Gui H, Xu DP, Yang YL, Su DF, et al. MicroRNA-124 mediates the cholinergic anti-inflammatory action through inhibiting the production of pro-inflammatory cytokines. *Cell Res.* 2013; 23: 1270-83.
27. Nakamachi Y, Ohnuma K, Uto K, Noguchi Y, Saegusa J, Kawano S. MicroRNA-124 inhibits the progression of adjuvant-induced arthritis in rats. *Ann Rheum Dis.* 2016; 75: 601-8.
28. Tang P, Xiong Q, Ge W, Zhang L. The role of microRNAs in osteoclasts and osteoporosis. *RNA Biol.* 2014; 11: 1355-63.
29. Yang M, Feng X, Ding J, Chang F, Chen X. Nanotherapeutics relieve rheumatoid arthritis. *J Control Release.* 2017; 252: 108-24.
30. Roy K, Kanwar RK, Kanwar JR. Molecular targets in arthritis and recent trends in nanotherapy. *Int J Nanomedicine.* 2015; 10: 5407-20.
31. Dolati S, Sadreddini S, Rostamzadeh D, Ahmadi M, Jadidi-Niaragh F, Yousefi M. Utilization of nanoparticle technology in rheumatoid arthritis treatment. *Biomed Pharmacother.* 2016; 80: 30-41.
32. Paulos CM, Turk MJ, Breur GJ, Low PS. Folate receptor-mediated targeting of therapeutic and imaging agents to activated macrophages in rheumatoid arthritis. *Adv Drug Deliv Rev.* 2004; 56: 1205-17.
33. Poh S, Chelvam V, Kelderhouse LE, Ayala-Lopez W, Vaitilingam B, Putt KS, et al. Folate-conjugated liposomes target and deliver therapeutics to immune cells in a rat model of rheumatoid arthritis. *Nanomedicine (Lond).* 2017; 12: 2441-51.
34. Yang M, Chang F, Ding J, Wang J, Gao Z, Zhuang X, et al. Scavenger receptor-targeted dextran sulfate-methotrexate prodrug for treatment of collagen-induced arthritis. *J Control Release.* 2017; 259: e98.
35. Yang M, Ding J, Feng X, Chang F, Wang Y, Gao Z, et al. Scavenger Receptor-Mediated Targeted Treatment of Collagen-Induced Arthritis by Dextran Sulfate-Methotrexate Prodrug. *Theranostics.* 2017; 7: 97-105.
36. Shin JM, Kim SH, Thambi T, You DG, Jeon J, Lee JO, et al. A hyaluronic acid-methotrexate conjugate for targeted therapy of rheumatoid arthritis. *Chem Commun.* 2014; 50: 7632-5.
37. Yu C, Li X, Hou Y, Meng X, Wang D, Liu J, et al. Hyaluronic Acid Coated Acid-Sensitive Nanoparticles for Targeted Therapy of Adjuvant-Induced Arthritis in Rats. *Molecules.* 2019; 24: 146.
38. Udalova IA, Mantovani A, Feldmann M. Macrophage heterogeneity in the context of rheumatoid arthritis. *Nat Rev Rheumatol.* 2016; 12: 472-85.
39. Low PS, Henne WA, Doorneweerd DD. Discovery and development of folic-acid-based receptor targeting for imaging and therapy of cancer and inflammatory diseases. *Acc Chem Res.* 2008; 41: 120-9.
40. Paulos CM, Varghese B, Widmer WR, Breur GJ, Vlashi E, Low PS. Folate-targeted immunotherapy effectively treats established adjuvant and collagen-induced arthritis. *Arthritis Res Ther.* 2006; 8: R77.
41. Nogueira E, Gomes AC, Preto A, Cavaco-Paulo A. Folate-targeted nanoparticles for rheumatoid arthritis therapy. *Nanomedicine.* 2016; 12: 1113-26.
42. Thomas TP, Goonewardena SN, Majoros JJ, Kotlyar A, Cao Z, Leroueil PR, et al. Folate-targeted nanoparticles show efficacy in the treatment of inflammatory arthritis. *Arthritis Rheum.* 2011; 63: 2671-80.
43. Yang C, Gao S, Kjems J. Folic acid conjugated chitosan for targeted delivery of siRNA to activated macrophages in vitro and in vivo. *J Mater Chem B.* 2014; 2: 8608-15.
44. Rollett A, Reiter T, Nogueira P, Cardinale M, Loureiro A, Gomes A, et al. Folic acid-functionalized human serum albumin nanocapsules for targeted drug delivery to chronically activated macrophages. *Int J Pharm.* 2012; 427: 460-6.
45. Zhao J, Zhao M, Yu C, Zhang X, Liu J, Cheng X, et al. Multifunctional folate receptor-targeting and pH-responsive nanocarriers loaded with methotrexate for treatment of rheumatoid arthritis. *Int J Nanomedicine.* 2017; 12: 6735-46.
46. Yang M, Ding J, Zhang Y, Chang F, Wang J, Gao Z, et al. Activated macrophage-targeted dextran-methotrexate/folate conjugate prevents deterioration of collagen-induced arthritis in mice. *J Mater Chem B.* 2016; 4: 2102-13.
47. Yang M, Chang F, Ding J, Gao Z, Zhuang X, Chen X. Treatment of collagen-induced arthritis by activated macrophage-targeted dextran-methotrexate/folate conjugate. *Nanomedicine.* 2018; 14: 1815-6.
48. Canal F, Sanchis J, Vicent MJ. Polymer-drug conjugates as nano-sized medicines. *Curr Opin Biotechnol.* 2011; 22: 894-900.
49. Marasini N, Haque S, Kaminskas LM. Polymer-drug conjugates as inhalable drug delivery systems: A review. *Curr Opin Colloid Interface Sci.* 2017; 31: 18-29.
50. Duncan R. Polymer conjugates as anticancer nanomedicines. *Nat Rev Cancer.* 2006; 6: 688-701.
51. Greco F, Vicent MJ. Combination therapy: Opportunities and challenges for polymer-drug conjugates as anticancer nanomedicines. *Adv Drug Deliv Rev.* 2009; 61: 1203-13.
52. Wong PT, Choi SK. Mechanisms and implications of dual-acting methotrexate in folate-targeted nanotherapeutic delivery. *Int J Mol Sci.* 2015; 16: 1772-90.
53. Thomas TP, Huang B, Choi SK, Silpe JE, Kotlyar A, Desai AM, et al. Polyvalent dendrimer-methotrexate as a folate receptor-targeted cancer therapeutic. *Mol Pharm.* 2012; 9: 2669-76.
54. Huang B, Otis J, Joice M, Kotlyar A, Thomas TP. PSMA-targeted stably linked "dendrimer-glutamate urea-methotrexate" as a prostate cancer therapeutic. *Biomacromolecules.* 2014; 15: 915-23.
55. Dang W, Colvin OM, Brem H, Saltzman WM. Covalent coupling of methotrexate to dextran enhances the penetration of cytotoxicity into a tissue-like matrix. *Cancer Res.* 1994; 54: 1729-35.
56. van Dongen MA, Rattan R, Silpe J, Dougherty C, Michmerhuizen NL, Van Winkle M, et al. Poly(amidoamine) dendrimer-methotrexate conjugates: the mechanism of interaction with folate binding protein. *Mol Pharm.* 2014; 11: 4049-58.
57. Nogueira E, Sarria MP, Azoia NG, Antunes E, Loureiro A, Guimaraes D, et al. Internalization of Methotrexate Conjugates by Folate Receptor-alpha. *Biochemistry.* 2018; 57: 6780-6.
58. Nakashima-Matsushita N, Homma T, Yu S, Matsuda T, Sunahara N, Nakamura T, et al. Selective expression of folate receptor beta and its possible role in methotrexate transport in synovial macrophages from patients with rheumatoid arthritis. *Arthritis Rheum.* 1999; 42: 1609-16.
59. Qi R, Majoros I, Misra AC, Koch AE, Campbell P, Marotte H, et al. Folate Receptor-Targeted Dendrimer-Methotrexate Conjugate for Inflammatory Arthritis. *J Biomed Nanotechnol.* 2015; 11: 1431-41.
60. Oh YK, Suh D, Kim JM, Choi HG, Shin K, Ko JJ. Polyethylenimine-mediated cellular uptake, nucleus trafficking and expression of cytokine plasmid DNA. *Gene Ther.* 2002; 9: 1627-32.
61. Boussif O, Lezoualc'h F, Zanta MA, Mergny MD, Scherman D, Demeneix B, et al. A versatile vector for gene and oligonucleotide transfer into cells in culture and in vivo: polyethylenimine. *Proc Natl Acad Sci U S A.* 1995; 92: 7297-301.
62. von Harpe A, Petersen H, Li YX, Kissel T. Characterization of commercially available and synthesized polyethylenimines for gene delivery. *J Control Release.* 2000; 69: 309-22.
63. Dong D-W, Xiang B, Gao W, Yang Z-Z, Li J-Q, Qi X-R. pH-responsive complexes using prefucosylated polymers for synchronous delivery of doxorubicin and siRNA to cancer cells. *Biomaterials.* 2013; 34: 4849-59.
64. Xu C, Wang P, Zhang J, Tian H, Park K, Chen X. Pulmonary Codelivery of Doxorubicin and siRNA by pH-Sensitive Nanoparticles for Therapy of Metastatic Lung Cancer. *Small.* 2015; 11: 4321-33.
65. Xie J, Teng L, Yang Z, Zhou C, Liu Y, Yung BC, et al. A polyethylenimine-linoleic acid conjugate for antisense oligonucleotide delivery. *Biomed Res Int.* 2013; 2013: 710502.
66. Teng LS, Xie J, Teng LR, Lee RJ. Enhanced siRNA Delivery Using Oleic Acid Derivative of Polyethylenimine. *Anticancer Res.* 2012; 32: 1267-71.
67. Patri AK, Kukowska-Latallo JF, Baker JR, Jr. Targeted drug delivery with dendrimers: comparison of the release kinetics of covalently conjugated drug

- and non-covalent drug inclusion complex. *Adv Drug Deliv Rev.* 2005; 57: 2203-14.
68. Kolate A, Baradia D, Patil S, Vhora I, Kore G, Misra A. PEG - a versatile conjugating ligand for drugs and drug delivery systems. *J control release.* 2014; 192: 67-81.
69. Takayanagi H. Osteoimmunology: shared mechanisms and crosstalk between the immune and bone systems. *Nat Rev Immunol.* 2007; 7: 292-304.
70. Takayanagi H, Kim S, Koga T, Nishina H, Isshiki M, Yoshida H, et al. Induction and activation of the transcription factor NFATc1 (NFAT2) integrate RANKL signaling in terminal differentiation of osteoclasts. *Dev Cell.* 2002; 3: 889-901.
71. Cheng CJ, Tietjen GT, Saucier-Sawyer JK, Saltzman WM. A holistic approach to targeting disease with polymeric nanoparticles. *Nat Rev Drug Discov.* 2015; 14: 239-47.
72. Poh S, Chelvam V, Low PS. Comparison of nanoparticle penetration into solid tumors and sites of inflammation: studies using targeted and nontargeted liposomes. *Nanomedicine.* 2015; 10: 1439-49.
73. Weissleder R, Nahrendorf M, Pittet MJ. Imaging macrophages with nanoparticles. *Nat Mater.* 2014; 13: 125-38.
74. Bendele A. Animal models of rheumatoid arthritis. *J Musculoskelet Neuronal Interact.* 2001; 1: 377-85.
75. Carlson RP, Datko LJ, O'Neill-Davis L, Blazek EM, DeLustro F, Beideman R, et al. Comparison of inflammatory changes in established type II collagen- and adjuvant-induced arthritis using outbred Wistar rats. *Int J Immunopharmacol.* 1985; 7: 811-26.
76. McInnes IB, Schett G. Cytokines in the pathogenesis of rheumatoid arthritis. *Nat Rev Immunol.* 2007; 7: 429-42.
77. Mateen S, Zafar A, Moin S, Khan AQ, Zubair S. Understanding the role of cytokines in the pathogenesis of rheumatoid arthritis. *Clin Chim Acta.* 2016; 455: 161-71.
78. Feng N, Yang M, Feng X, Wang Y, Chang F, Ding J. Reduction-Responsive Polypeptide Nanogel for Intracellular Drug Delivery in Relieving Collagen-Induced Arthritis. *ACS Biomater Sci Eng.* 2018; 4: 4154-62.
79. Fung WP, Przybylski M, Ringsdorf H, Zaharko DS. In vitro inhibitory effects of polymer-linked methotrexate derivatives on tetrahydrofolate dehydrogenase and murine L5178Y cells. *J Natl Cancer Inst.* 1979; 62: 1261-4.
80. Lee DJ, Kessel E, Edinger D, He D, Klein PM, Voith von Voithenberg L, et al. Dual antitumoral potency of EG5 siRNA nanoplexes armed with cytotoxic bifunctional glutamyl-methotrexate targeting ligand. *Biomaterials.* 2016; 77: 98-110.
81. Jia M, Li Y, Yang X, Huang Y, Wu H, Huang Y, et al. Development of both methotrexate and mitomycin C loaded PEGylated chitosan nanoparticles for targeted drug codelivery and synergistic anticancer effect. *ACS Appl Mater Interfaces.* 2014; 6: 11413-23.
82. Southan C. A genomic perspective on human proteases as drug targets. *Drug Discov Today.* 2001; 6: 681-8.
83. Wosikowski K, Biedermann E, Rattel B, Breiter N, Jank P, Loser R, et al. In vitro and in vivo antitumor activity of methotrexate conjugated to human serum albumin in human cancer cells. *Clin Cancer Res.* 2003; 9: 1917-26.
84. Garg NK, Tyagi RK, Singh B, Sharma G, Nirbhavane P, Kushwah V, et al. Nanostructured lipid carrier mediates effective delivery of methotrexate to induce apoptosis of rheumatoid arthritis via NF-kappaB and FOXO1. *Int J Pharm.* 2016; 499: 301-20.
85. Burmester GR, Pope JE. Novel treatment strategies in rheumatoid arthritis. *The Lancet.* 2017; 389: 2338-48.